

Investigating the Flow Behaviour of CO₂ and N₂ in Porous Medium Using Core Flooding Experiment

Nuhu Mohammed*, Abubakar J. Abbas, Godpower C. Enyi, Muhammad Kabir Abba, Onukak Imeh Etim, Bello Saidu, Salihu M. Suleiman, Hassan Kabiru Yar'adua

*Corresponding author: (n.mohammed5@edu.salford.ac.uk)

Abstract

Several researchers employed N₂ to augment CH₄ recovery efficiency and CO₂ sequestration during the Enhanced Gas Recovery (EGR) process in consolidated rocks. To our knowledge, there has been limited data backing the reason why CO₂ experienced a more extended breakthrough during the EGR process in the presence of N₂ gas. This study investigated CO₂ and N₂ behaviour during the core flooding experiment by CO₂ injection in Bentheimer core plug. N₂ was used as the continuous phase during the core flooding process, while CO₂ was the dispersed phase. The experiment was designed with varying injection rates at 30 and 40 °C temperature points. The experimental findings showed that the dispersion and diffusion coefficient, CO₂ storage, concentration profile and breakthroughs were highly influenced by temperature change, especially at lower injection rates. However, at high injections, those properties are less sensitive to change in temperature, with most of the curves overlapping in the concentration profile. The highest and most negligible dispersion and diffusion coefficients were recorded at the highest and lowest injection rates respectively. These results agree with those reported by several researchers for sandstone rocks. Thus, higher temperatures have a more substantial effect on dispersion and diffusion coefficient, which eventually led to higher mixing between CO₂ and N₂. The breakthrough time decreases with an increase in reservoir temperature, confirming the diffusion and dispersion coefficients are temperature dependent. The experiment at 30 °C recorded an extended breakthrough time over that at 40 °C. The maximum breakthrough time at 0.52 PV was recorded at 30 °C at the lowest injection rate. The concentration profile highlighted the trend between the displacing and displaced gas during the core flooding experiment. From the range of injections and temperatures tested, the CO₂ PV stored decreases as the rate of injection increases from 0.4 – 1.2 ml/min. However, the CO₂ stored was more promising at higher rates, corresponding with high differential pressure, due to flow resistance within the tortuous flow channels in the porous medium.

Keywords: Diffusion coefficient; pore volume; CO₂ sequestration, mixing, dispersion coefficient

1. Introduction

Gas transport in porous media occurs in different applications, including catalytic converters, fuel cells, oil and gas exploration, carbons storage, and the food processing industry, to mention a few (Abba et al., 2018). More so, to design and optimize a specific process that involves the transport of gases in porous media, there is a need to thoroughly understand the interplay mechanism for such gas as they meet each other. This gas transport is based on various empirical models developed to optimize and evaluate the design and performance of the processes (Abba et al., 2018). This research emphasized more on gas transport as against vapour transport unless otherwise stated therein. The best way to separate gas from vapour was based on their physical states at the standard condition of temperature and pressure of 20 °C and 1 bar, respectively, (Molly & Mark, 2006). The analytical conditions of CO₂, N₂ and CH₄, are 31.05 and 73.80, -146.9 and 33.90, 82.55 °C and 46 bars for temperature and pressure respectively. Although this can only be applied if the gas components remain liquid at normal temperature and pressure, such fluid is considered a vapour or condensate. However, if the gas components remain as gaseous and not condensable at standard temperature and pressure, such fluid is regarded as a gas. This distinct phenomenon is essential as it provides a clear understanding of the two primary transport mechanisms affecting the flow behaviour of gases and vapours through the porous media. These factors are diffusion and dispersion processes with more focus on the dispersion dominant porous media transport mechanism, being critical in determining the extent of CO₂ or N₂ with the nascent CH₄ during the EGR process by gas alternating gas injection.

Thus, in turn, to successfully optimise and reduce the overhead cost of exploring residual natural gas during the EGR process, the mode of displacing gases needs to be comprehensively investigated in order to avoid premature mixing. Such premature mixing primarily arises from several core sample property parameters. These are longitudinal dispersion coefficient, mobility ratio, porosity, permeability, dispersivity, viscous fingering, gravity, flow velocity, diffusion coefficient, and the likes. The viscosity ratio measures mobility. This is similar to the case of supercritical carbon dioxide displacing methane. The CO₂ is denser than either N₂ or CH₄ at conditions relevant to the EGR process, i.e. $\frac{\mu_{CH_4}}{\mu_{CO_2}} < \frac{\mu_{N_2}}{\mu_{CO_2}} < 1$.

The flow mechanism of supercritical carbon dioxide as it moves transverses the pore sizes of the Bentheimer core plug to displace the continuous natural phase is quite complicated, particularly in the presence of nitrogen as booster gas. Studying such a complex phenomenon is vital to understanding the patterns and expected outputs of the displacement process. These gases mostly exhibit liquid density while still retaining the gas viscosity at their supercritical state.

Several researchers have studied the dispersion and diffusion mechanism during the EGR process in a porous medium. For example, in (1988), Newberg used an explicit variety of sandstone plugs to measure the CH₄ and N₂ scale of mixing. The experiment was conducted at varying flow velocities of 0.02-0.3mm/s and 34.5 to 68.9 bars of pressure. In addition, an enhanced gas recovery by CO₂ flooding in dry carbonate sandstone plugs was investigated (Seo, 2004; Seo and Mamora, 2005). The distribution of CH₄ and CO₂ molecules at the breakthrough time was examined using Computed Tomography (CT). The dispersion coefficient was also measured, and 73-87% CH₄ recovery was recorded. Furthermore, Hughes et al. (2012) studied the reaction of different CH₄ and CO₂ longitudinal dispersion coefficient elements using consolidated sandstones. The experiment was carried out under a wide range of permeabilities. A lower displacement velocity in the horizontal direction shows a significant gravitational effect on the rocks with higher permeability. At the same time, the dispersion coefficient was 63% more than the nascent value due to the gravitational effect. More so, Abba et al. (2018), at 95 bars and 40 °C of pressure and temperature, studied the impact of connate-water salinity on the Berea grey core dispersion mechanism.

The novelty of this work was the use of inert N₂ gas as external support for simultaneous CH₄ recovery and CO₂ storage improvement. The experimental results have proven that N₂ can be used as third-party gas to improve natural gas recovery and CO₂ storage during the EGR process. However, the mechanism behind such improvement is limited, which was this study's focus solely to investigate that effect. Furthermore, to our knowledge, there have been limited data backing the reason why CO₂ experienced a more extended breakthrough during the EGR process in the presence of N₂ gas using consolidated sandstone rocks. Therefore, this study is designed to establish why CO₂ experiences a more extended breakthrough during the Enhanced Gas Recovery (EGR) process with N₂ booster gas.

To date, there are limited experimental data on how the displacing and displaced fluids interact during the core flooding displacement process. This paper investigates CO₂ and N₂ behaviour during core flooding experiments by CO₂ injection in a *Bentheimer* core plug. N₂ was used as the continuous phase (saturating fluid) during the core flooding process, while CO₂ was the dispersed phase (displacing). This study was primarily designed to establish why CO₂ experiences a more extended breakthrough time during Enhanced Gas Recovery (EGR) process (Mohammed et al., 2021) with N₂ as the displaced gas. The experiment was designed with varying injection rates at 30 and 40 °C temperature points. Thus, for this study, the operation conditions are at average normal reservoir pressure of 0.1 bar/m gradients, 1000m depth, and 30-40 °C/1000m temperature gradient, which is well above each single gas species criticality.

2. Advection vs Diffusion

Transport systems in the environment may be classified into two types. These are advection and diffusion. Advection refers to movement with the mean fluid flow. In contrast, diffusion assigns to the bulk transfer of compounds through

the means of random motions. In addition, diffusion isolates sharp discontinuities in concentration and results in smoother, flatter, and precise concentration profiles (Mass Transport Processes, 2021).

In this paper, Eqs. 1-8 was developed to model and evaluate the dispersion driving mechanism. These fundamental equations were originated based on several works of literature as outlined by (Abba et al., 2017; Abba et al., 2018; Abba et al., 2019; Takahashi & Iwasaki, 1970; Fuller et al., 1966; Newberg & Foh, 1988; Hughes et al., 2012; Mammora and Seo, 2002; Liu et al., 2015; Perkins & Johnston, 1963; Coats et al., 2009; Honari et al., 2013). More information can be obtained in our initial publications (Mohammed et al., 2019; Mohammed et al., 2020).

$$K_L \frac{\partial^2 C}{\partial x^2} - u \frac{\partial C}{\partial x} = \frac{\partial C}{\partial t} \quad (1)$$

Also, Eq. (1) was further simplified into a dimensionless form, presented in Eq. (2).

$$\frac{1}{P_e} \frac{\partial^2 C}{\partial x_D^2} - \frac{\partial C}{\partial x_D} = \frac{\partial C}{\partial t_D} \quad (2)$$

Where,

Parameter	Symbol	Expression
Peclet number	P_e	$\frac{uL}{K_L}$
Dimensionless time	t_D	$\frac{tu}{L}$
Dimensionless distance	x_D	$\frac{x}{L}$
Interstitial velocity	u	$\frac{Q}{\pi r^2 \phi}$

The solution of Eq. (2) was shown in Eq. (3) under a known initial ($C = 0$ at $t_D = 0$) and boundary conditions ($C = 1$ at $x_D = 0$, $C \rightarrow 0$ as $x_D \rightarrow \infty$)

$$C = \frac{1}{2} \left\{ \operatorname{erfc} \left(\frac{x_D - t_D}{2\sqrt{t_D/P_{em}}} \right) + e^{P_{em}x_D} \operatorname{erfc} \left(\frac{x_D + t_D}{2\sqrt{t_D/P_{em}}} \right) \right\} \quad (3)$$

The final longitudinal dispersion coefficient was determined by curve fitting the CO₂ exit composition (C) measured by the online GC into the 1AD equation. However, to forecast the dominant mechanism of displacement, the model equation governing the medium peclet number (P_{em}), the characteristic length scale of mixing (d), molecular diffusion coefficient (D) and mean interstitial velocity (um) was used as presented in Eq. (4).

$$P_{em} = \frac{u_m d}{D} \quad (4)$$

In general, when $P_{em} < 0.1$, the dominant mechanism within the porous medium is diffusion like, while the advective mixing becomes dominant at $P_{em} > 10$ (Perkins and Johnson, 1963). Also, an intermediate zone co-exists when the value of P_{em} ranges between 0.1-10.0. Thus, the model equation developed by Coast et al. (2009) was used to evaluate the dispersivity of the Bentheimer core sample.

$$\frac{K_l}{D} = \frac{1}{\tau} + \alpha \frac{u_m^n}{D} \quad (5)$$

Here α represent the Bentheimer core plug dispersivity in meters in the presence of an exponential constant (n). However, most consolidated sandstones have a tortuosity (τ) ranges between 1-13 (Honari et al., 2013). Thus, the tortuosity (τ) of the Bentheimer was evaluated as an intercept point (Hughes et al., 2012) obtained from the linear plot of Eq. (5).

Gas-phase diffusion is often assumed to be dominated by molecular diffusion. However, the irregular broadening of a solute along concentration gradients over time is described here by the one-dimensional Fick's second law presented in Eq. 6.

$$\frac{\partial C}{\partial t} = D_a \frac{\partial^2 C}{\partial x^2} \quad (6)$$

Where C is the gas concentration (mol/m³), t is time (s), D_a is the binary molecular diffusion coefficient of air (m²/s), and x is the distance along the axis of flow (m). When the main collision is within molecule-molecule interaction without colliding with the wall of the container, such a process is called molecular diffusion. More complex gas-phase diffusion processes can also occur in some situations, such as viscous, Knudsen, and non-equimolar diffusion (Scanlon et al., 2000). The former two processes are said to occur due to pore walls and resultant molecule-wall collisions (Cunningham and Williams, 1980). The latter requires both the presence of system walls and a multicomponent gas, and such conditions are primarily present in porous media and lead to digression from Fick's law (Sleep, 1998). Baehr and Bruell (1990) report that high vapour pressures, especially those near organic liquid sources, results in divergence from Fick's law. Diffusion is a solute-dependent component of dispersion due to the relationships among average kinetic energy, velocity, and molecular mass (Molly & Mark, 2006). Meanwhile, at a given temperature, the average kinetic energy of all gases is equal and presented in Eq. 7.

$$E_k = \frac{3}{2} kT = \frac{1}{2} m v_{rms}^2 \quad (7)$$

Where k is Boltzmann's constant (J-K⁻¹), T is the temperature (K), m is the solute mass (kg), and v_{rms} is the root-mean-square velocity of the gas particles (m/s). Thus, lower molecular weight gases are said to exhibit higher average velocities than those with a higher molecular weight under given thermal equilibrium and consequent equal kinetic energy (Molly & Mark, 2006). This higher velocity results in more significant diffusion coefficients, which grossly contributions to overall advection (dispersion) domination.

The widely accepted model equation, developed by Takahashi & Iwasaki in 1970 for diffusion coefficient evaluation, was used. Unfortunately, this model is primarily applicable for CO₂ and CH₄ systems. This necessitates the use of an alternative model equation developed by Fuller et al. (1966). This model can be relevant for CO₂ and N₂ displacement, as shown in Eq. 8.

$$D_{N_2, CO_2} = \frac{1.0110 \times 10^{-4} T^{1.75} \sqrt{(1/\mu_{N_2} + 1/\mu_{CO_2})}}{P[(\sum V_{N_2})^{1/3} + (\sum V_{CO_2})^{1/3}]^2} \quad (8)$$

The model equation was further simplified and expressed as equation (8b) substitution.

$$D_{CO_2, N_2} = \frac{7.69 \times 10^{-11} T^{1.75}}{P} \quad (8b)$$

In equation (8b) T and P are the experimental temperature and pressure in Kelvin (K) and MPa, respectively.

3. Materials and Methods

In this paper, N₂ and CO₂ behaviour were investigated using core flooding experiments with Bentheimer core plug. N₂ was used as the continuous phase during the core flooding process, while CO₂ was the dispersed phase. The

experiment was designed with varying injection rates at temperatures of 30 and 40 °C and 102 bars pressure. The general properties of the Bentheimer core plug used and the initial experimental conditions were shown in Table 1 and 2.

Table 1.

The characteristics of Bentheimer core plug at conditions relevant to the EGR process

Core plug	Length (m)	Diameter (m)	Porosity (%)	Gas Permeability (D)
Bentheimer gray	0.076	0.025	22.80	2.10

Table 2.

The initial experimental conditions relevant to the EGR process

Components	Value
Saturation gas	N ₂
Injection gas	CO ₂
Fluid composition, wt. %	99.9
Initial pressure, bars	102
Initial temperature, °C	30-40
Injection pressure, bars	100-102
Injection composition, wt. %	98-99
Production constraints, wt. %	Breakthrough @ 2-5% CO ₂ product contamination
Dispersion coefficient range, m ² /s	8-50 x10 ⁻⁸
Diffusion coefficient range, m ² /s	15-30 x10 ⁻⁸

Procedure

To achieve a negligible moisture content and volatile organic compounds (VOCs), the Bentheimer core plug was oven-dried at a temperature of 110 °C for 24 hours. Also, to maintain smooth and uniform gas molecule distribution and avoid permeation through the viton sleeve, the core plug was securely wrapped with a thread tape followed by aluminium foil before inserting into the resistance rubber sleeve. The overburden pressure was set at 170 bars, reasonably above the pore pressure to prevent the core sleeve from rupturing. More so, the temperature was set and maintained at 30 °C. The equipment lines were flooded with N₂ until the final composition attained was $\geq 98\%$ from the GC spectrum. A pressure leak test was carried out to ensure the system was leak-free. CO₂ was later injected at 0.4 ml/min using pump C/D and accumulator B, as shown in Fig. 1. At every 5 minutes sequential interval, the GC analyzed and recorded the endpoint concentration until CO₂ was dominant relative to N₂ (i.e. CO₂ composition > 98%). The experiment was terminated, and the lines were de-pressurized. Additional tests were further carried out at 0.6, 0.8, 1.0, and 1.3 ml/min using the same protocol as already described. Thus, to investigate the effect of temperature, similar sets of the experiment were conducted using a fresh core sample, but this time at a higher temperature of 40 °C while maintaining the same 102 bars pressure. The experimental flow diagram is presented in Fig. 1.

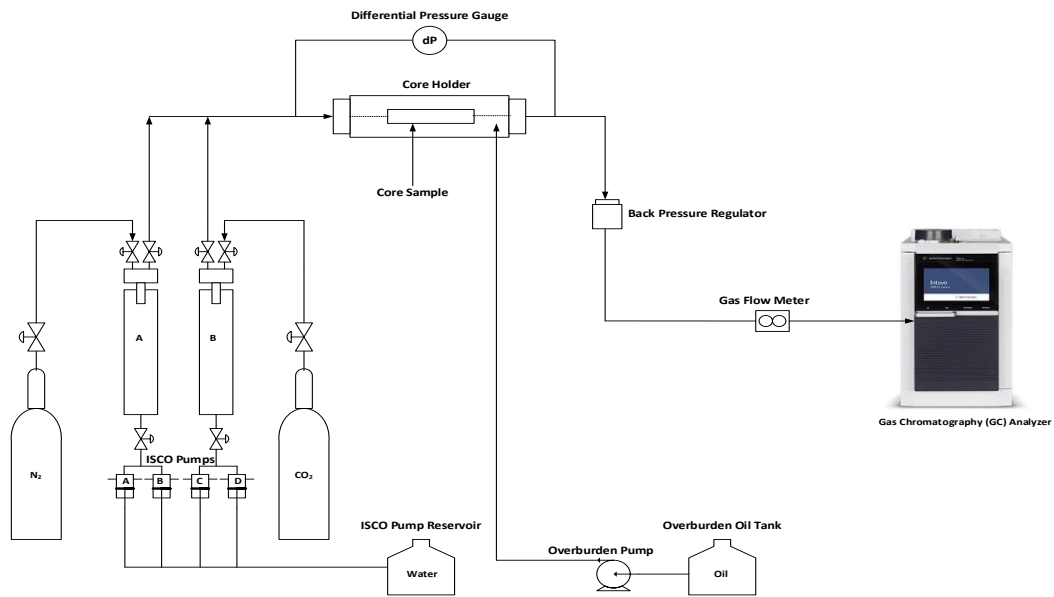


Fig. 1. Experimental flow diagram of N₂ displacement by CO₂ flooding

4. Results

4.1 Temperature effect on dispersion and diffusion coefficient

Sets of experiments were carried out in Bentheimer core samples to investigate the diffusion and dispersion coefficient dependence on temperature. The study was performed at 30 and 40 °C temperatures, 102 bars of pressure, at a specific CO₂ injection rate (0.4, 0.6, 0.8, 1.0, and 1.2 ml/min). Fig. 2 shows that the diffusion coefficient is directly proportional to temperatures, which conforms with the findings outlined by other researchers (Mamora and Seo, 2002; Liu et al., 2015; Mohammed et al., 2019; Abba et al., 2018). Thus, the molecular movement of the gas species is directly proportional to temperature due to the rise in activation energy. As the gas species move along the core, they slowly exceed the natural force of attraction between them as a result of elevated temperatures within the pore matrix. It gives them substantial liberation to flow over more significant space due to increased kinetic energy associated with temperature rise. Thus, it later promotes the free diffusion of CO₂ and N₂ molecules, resulting in more displacing and displaced gas molecules entering each other, affirming higher mixing scales. A piece of evidence was the plot of dispersion coefficient against injection rate in Fig. 3, with higher dispersion coefficient values at 40 than at 30 °C under the same range of CO₂ injection velocities. A combined average of 25% rise was recorded when the temperature increased from 30 to 40 °C. Therefore, the dispersion and diffusion coefficient increase due to temperature rise. It can be drawn that high temperature encouraged the mixing of gases under motion within the pore channels at simulated reservoir conditions. Therefore, gas fields with higher temperatures are likely unsuitable for the CO₂ enhanced gas recovery process for fundamental production operations. In general, the turbulence effect is undoubtedly responsible for high diffusion and dispersion along the core length due to increased flow velocities. In this study, the highest dispersion occurred at 1.2 ml/min while the least was recorded at 0.4 ml/min, as shown in Fig. 2.

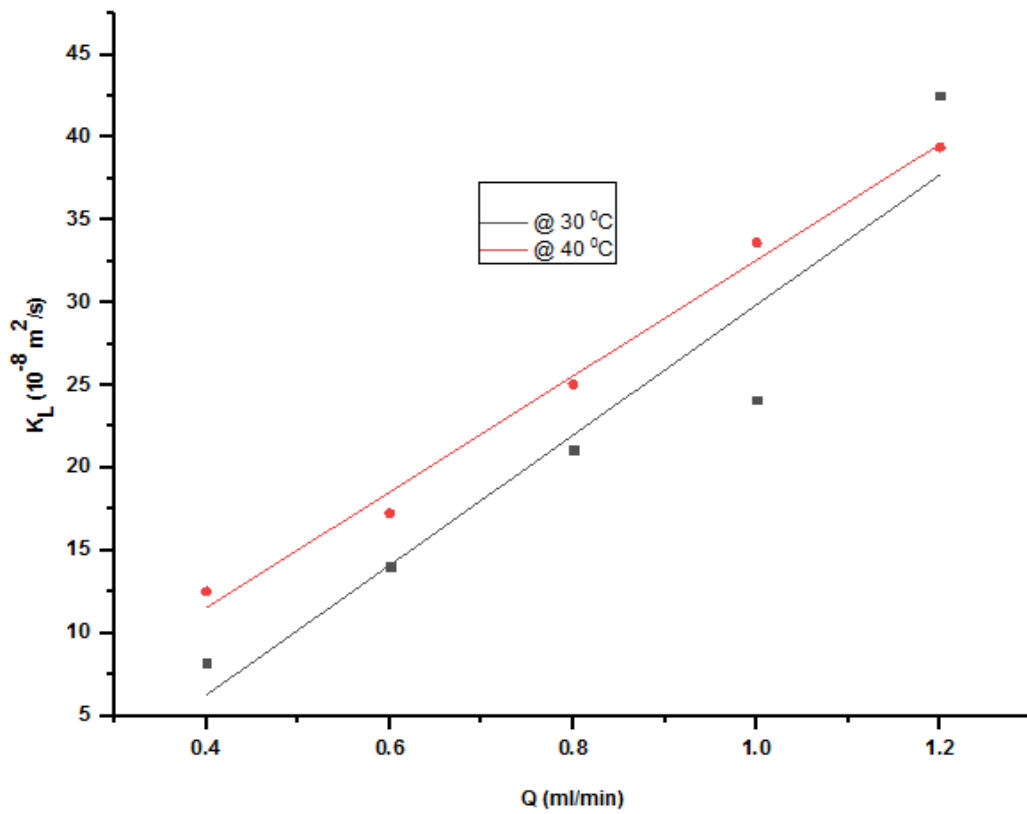


Fig. 2. Effect of injection rates on the longitudinal dispersion coefficient at 30 & 40 °C

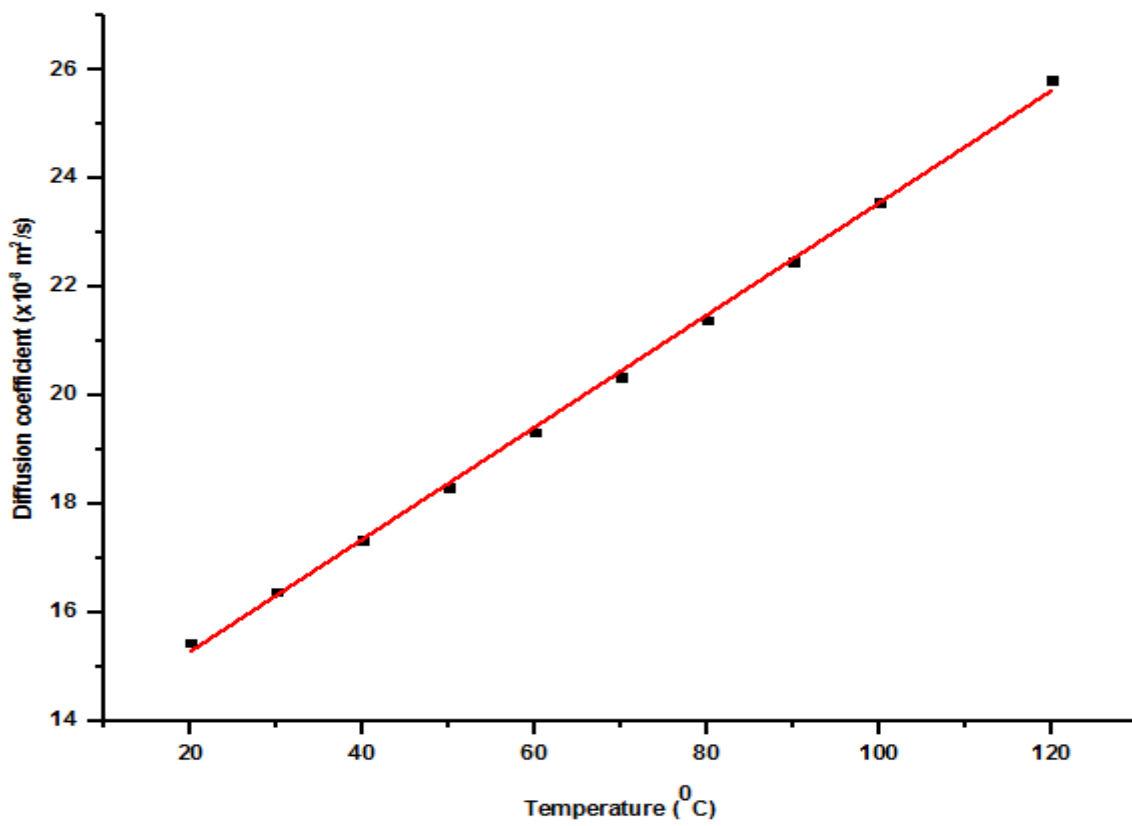


Fig. 3. Relationship between diffusion coefficient and temperature at 102 bars using Eq. (8b)

4.2 Effect of temperature on dispersivity

The experimental data at 30 and 40 °C were applied to evaluate the dispersivity (α) of the Bentheimer core plug using Eq. (4), at $\tau = 3, 2$ and $n = 1$. From Fig. 4 & 5, the dispersivities of the core plug were well fitted by experimental results at 30 and 40 °C. More so, the medium pecelet number Pe_m at 40 °C was calculated to be 0.964 – 2.894. In addition, a moderate convection effect was observed at lower injection velocities (0.06-0.09 mm/s), corresponding to 0.964 – 1.448 medium pecelet number range, with diffusion being the dominant mechanism. As the injection velocity further rises with a corresponding medium pecelet number range of 1.448 – 2.89, the convection effect intensifies. Thus, both diffusion and convection dominated the process, resulting in early CO₂ breakthroughs. Therefore, selecting the correct injection rate is vital for simultaneous CO₂ storage and the EGR process. The dispersivity (α) for the core plug at 30 °C was recorded as 0.00265 m, less than those reported by (Mohammed et al., 2020; Abba et al., 2018) and within the range written by (Gist et al., 1990; Schulze-Makuch, 2005; Honari et al., 2013). In summary, the application of Eq. (4) to the experimental results permit the dispersivity (α) to be evaluated for the two temperatures considered for the Bentheimer sandstone plug. For 30 and 40 °C of temperature, $\alpha = 0.00222$, and 0.002265 m, and these results are within the range reported for sandstones by (Coats et al., 2009; Schulze-Makuch, 2005; Liu et al., 2020), although for the 40 °C temperature, the dispersivity recorded was slightly higher, though lower than that presented according to (Brigham et al., 1974). Thus, higher temperatures have a more substantial effect on dispersion and diffusion coefficient, which eventually led to mixing CO₂ and N₂ from a more significant perspective (Liu et al., 2018).

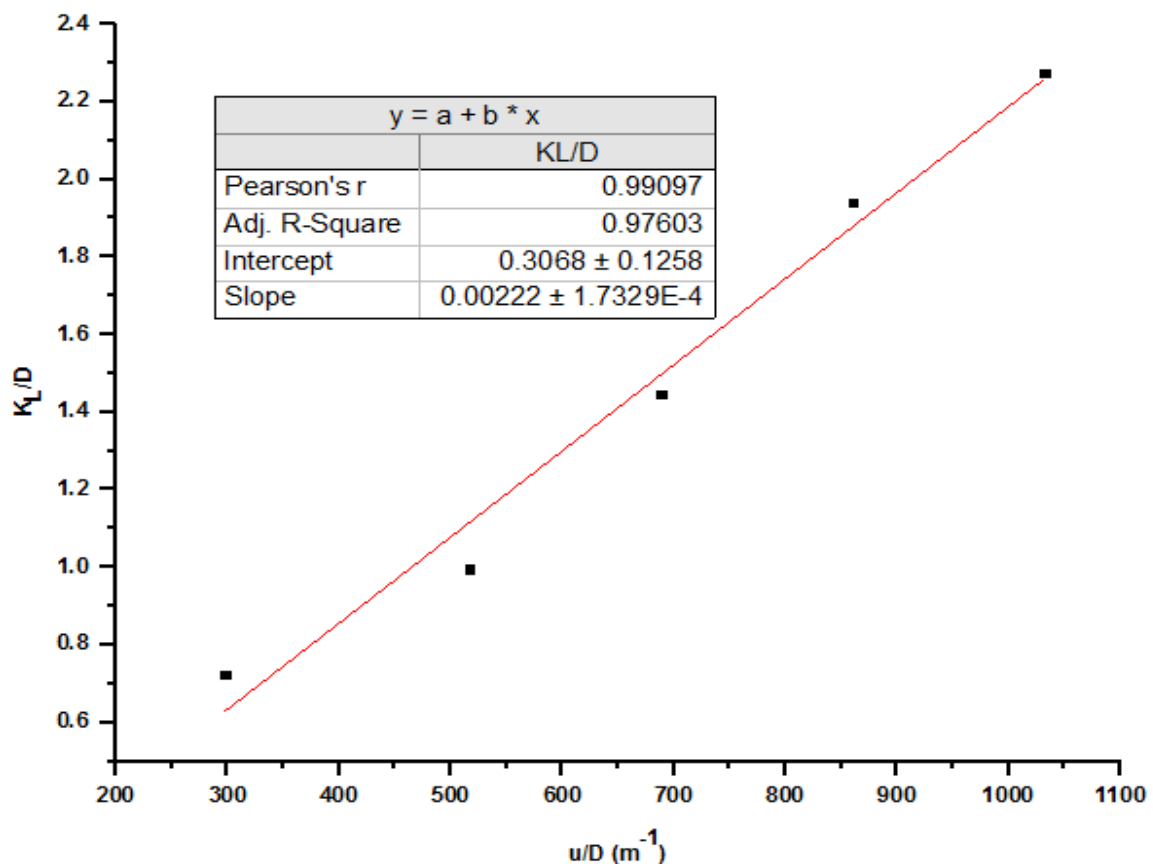


Fig. 4. Plot of dispersivity determination at 30 °C

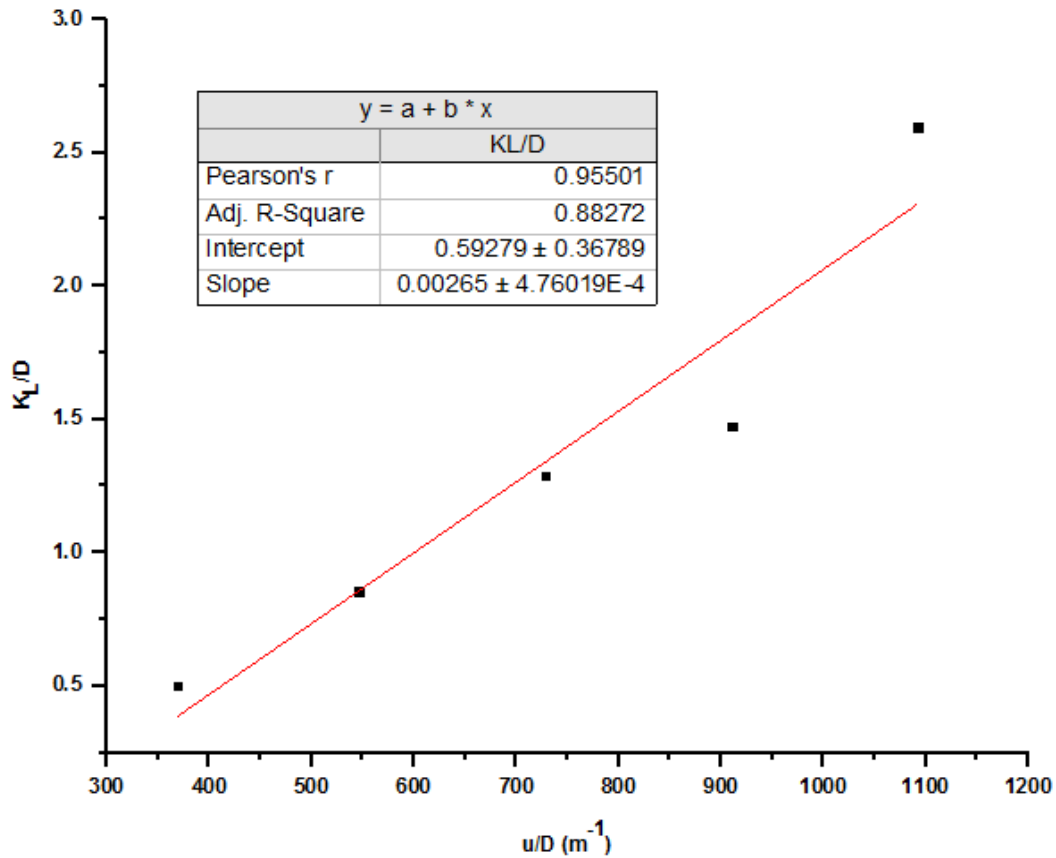


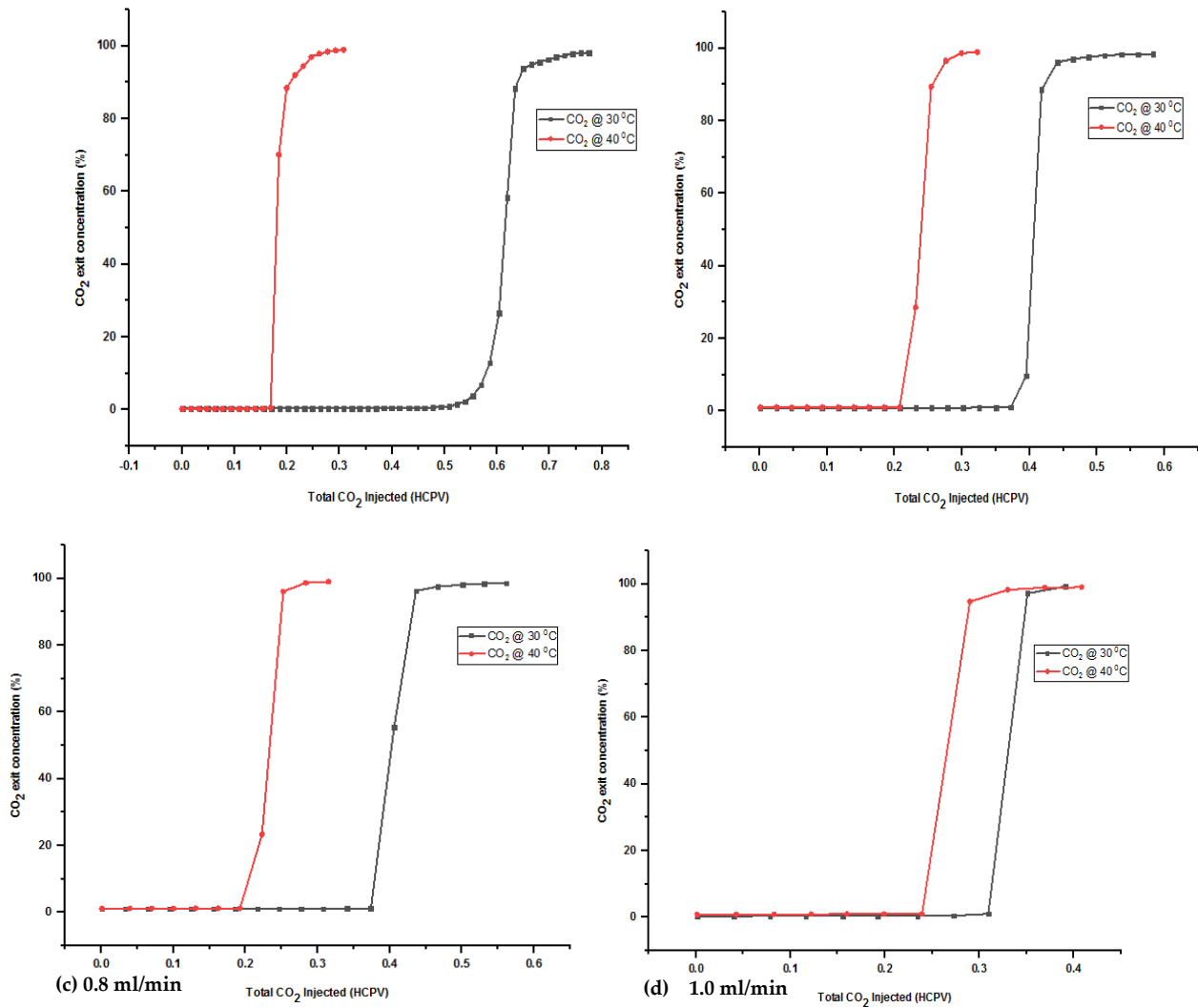
Fig. 5. Plot of dispersivity determination at 40 °C

4.3 CO₂ breakthrough

The breakthrough is considered as a point at which the displacing gas (CO₂ or N₂ gas) was noticed at the exit product stream. In this study, the breakthrough was characterised within 1-3% CH₄ contamination by CO₂, in other words, when the GC output indicated CO₂ concentration within a range of 1-3% concentration. The CO₂ breakthrough curves (S-shape curves) were obtained by plotting CO₂ mole fractions at the exit stream against the PV of injected CO₂. The experiment was carried out at two temperature regimes (30 and 40 °C) to investigate the influence of temperature variation on CO₂ breakthrough at different injection velocities. The CO₂ breakthrough tailed off with reservoir temperature rise, signifying the dependence of diffusion and dispersion coefficients on temperature. The experiment at 30 °C recorded an extendable breakthrough time than that at 40 °C in all cases. The maximum breakthrough at 0.52 PV was recorded at 30 °C and the lowest injection velocity. The breakthrough, however, decreased to 0.17 PV when the temperature increases from 30 to 40 °C. The breakthrough curves recorded at 30 °C are less steep compared with those measured at 40 °C. Figs. 6a-e present the CO₂ breakthroughs at varying injection rates for 30 and 40 °C experimental conditions. These graphs were obtained by plotting the CO₂ exit composition from the downstream of the core holder by GC equipment against the injected PV of CO₂. At a lower injection rate, the temperature effect was quite significant, as observed from the vertical distance difference of the two plots. Thus, at lower injection, the temperature effect was the driving factor compared to the injection rates. However, as the injection rates increase from 0.4-1.2 ml/min, such vertical differences become minimal until at 1.2 ml/min when the two plots (30 and 40 °C) overlap. At this point, the injection rate effect overcomes the dominant temperature effect and became the dominant driving factor. The experiments were carried out at constant pressure of 102 bars and an interstitial velocity range of 0.06 – 0.18 mm/s.

The most extended CO₂ breakthrough at 0.52 PV was noticed at 0.06 mm/s and 30 °C, which later tailed off by 50% when the interstitial velocity increase to 0.18 mm/s. The least CO₂ breakthrough at 0.17 PV was observed at 0.06 mm/s

and 40 °C temperature. Ostensibly, at this conditions, the highest injected CO₂ (0.8 PV) through the system was recorded during the displacement experiment. These results are in agreement with the study reported by (Mesfer et al., 2020). Overall, the gas injection velocity has a strong influence in determining the CO₂ breakthrough point and are more significant at lower rates. As evidenced in Fig. 6a-e, when the change in the breakthrough periods between the two sets of temperature decreases from 0.35 PV to nearly zero. The two plots in Fig. 6e overlap with each other, recording the same breakthrough period at 0.24PV. Thus, a prolonged CO₂ breakthrough signifies lower mixing and higher storage at reduced system temperature where diffusion dominates. In contrast, the gas molecules gain higher kinetic energy at higher injections rates sufficient enough to create turbulent flow regime. Hence, making advection dominant as against diffusion within the porous medium.



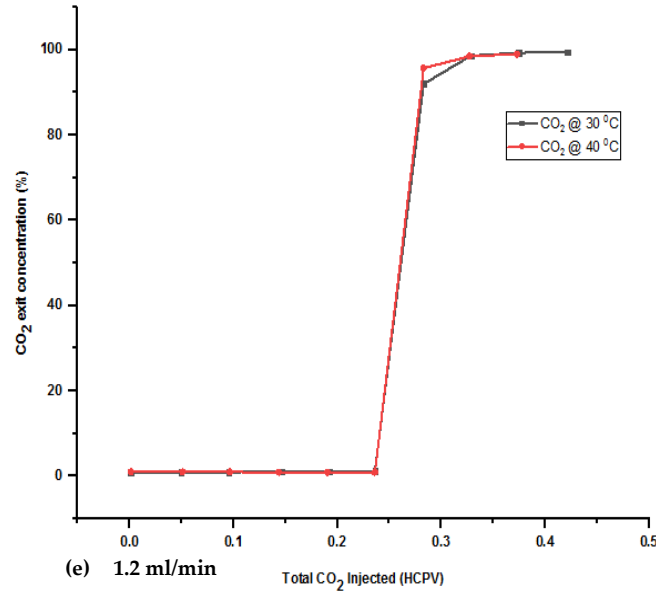


Fig. 6a-e. CO₂ breakthrough at varying injection rate (0.4-1.2 ml/min) for 30 & 40 °C temperatures.

Diffusion is highly temperature-dependent, meaning the higher the temperature, the higher the rate of diffusion. Higher temperatures promote faster movement of the gas species within the porous medium due to the increase in their respective kinetic energies. This means only fewer molecules of the CO₂ would have sufficient kinetic energy to contact the N₂ in the outlet stream of the core holder, which is why lower amount of CO₂ was recorded before breakthrough at lower injections. Thus, CO₂ injected sinks to the lower part of the porous medium, indirectly influencing higher storage in the context of geological sequestration and apparently, less effluent contamination. In summary, the lower the temperature, the lower the mixing (lower dispersion coefficient), the longer the CO₂ breakthrough and invariably better storage with little product contamination.

4.4 Concentration profile

The concentration profile plots highlight the trend between the displacing and displaced gas during the core flooding experiment. These plots were presented in Figs. 7a-e. According to Fig. 7a, as the PV of the total injected CO₂ reaches 0.17 PV, a current of CO₂ was detected at the exit stream, which invariably indicates the presence of a displacement front. After this, the exit CO₂ concentration increases linearly with the total CO₂ injected (HCPV) until it reaches the peak at nearly 0.3 PV, corresponding to approximately 0.99 CO₂ mole fraction. At this point, an insignificant concentration of N₂ was recorded at the downstream of the core holder depicted by the green curve in Fig. 7a. Thus, indicating a significant recovery of the N₂ has occurred.

A similar trend was observed when the experiment was carried out at a higher temperature of 40 °C. Thus, a point of intersection was observed at almost 50% of the CO₂ exit concentration at 30 and 40 °C. Furthermore, the curves at 30 °C were steeper than at 40 °C, indicating higher extent of mixing between the N₂ and CO₂. This was evident later in Table 2, with most of the runs at 40 °C recording a higher value of dispersion coefficient under the same injection scenarios. More so, when the injection rate increases from 0.4 – 1.2 ml/min, the distance between the two intersection of curves decrease until it becomes less visible, especially at the maximum injection of 1.2 ml/min. At this point, the N₂ and CO₂ curves overlapped, as shown in Fig. 7e. Such plot was in synergy with the breakthrough plot in Fig. 6e. Thus, it can be deduced that as the interstitial velocity increases during the EGR process, both N₂ and CO₂ experienced similar phase change behaviour under reservoir conditions.

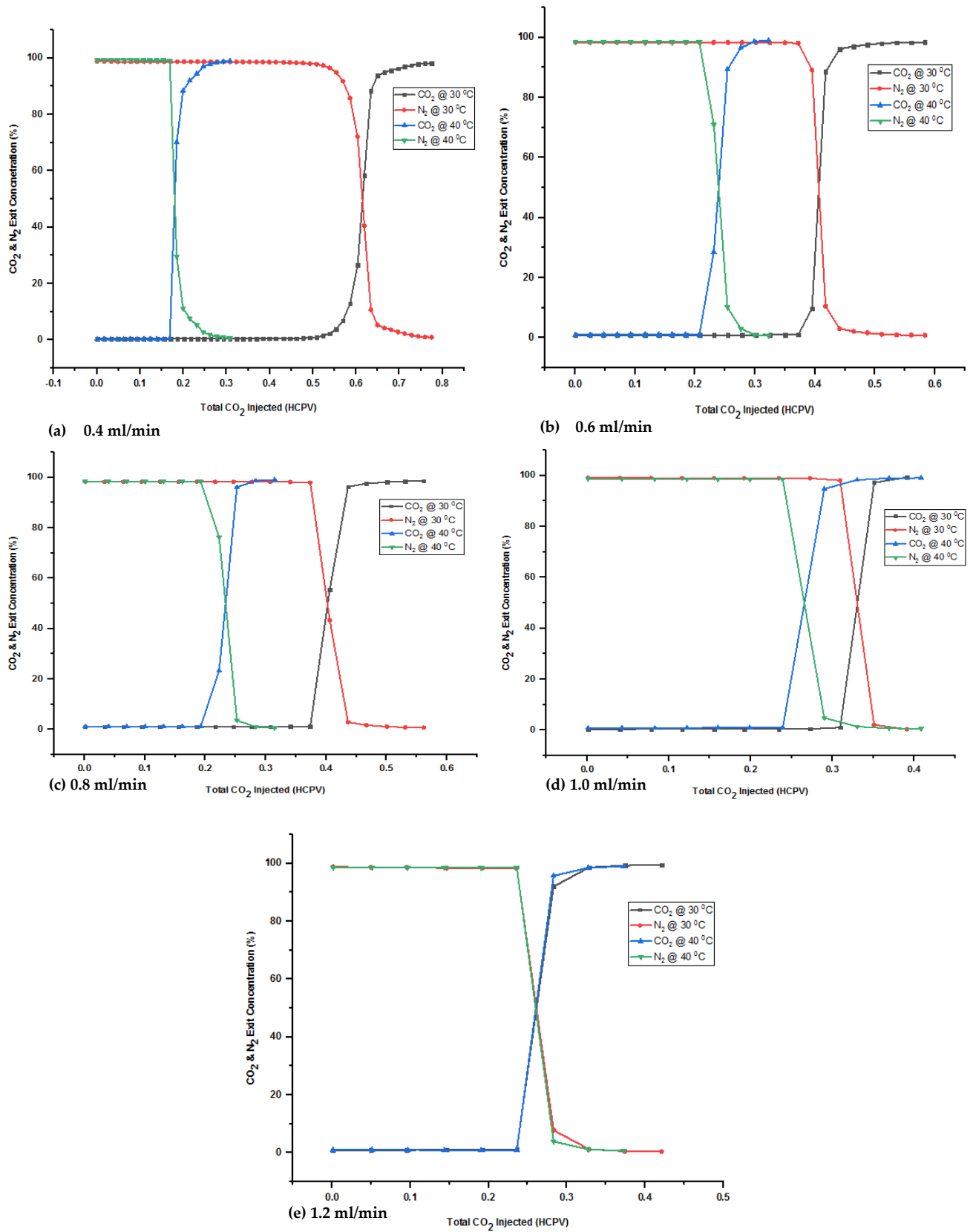


Fig. 7a-e. Concentration profile at varying injection rate (0.4-1.2 ml/min) for 30 & 40 °C temperatures.

4.5 CO₂ sequestration

The CO₂ sequestration was examined using the law of mass conservation as demonstrated by Abba et al. (2018). As a result, the total amount of CO₂ injected and produced can be determined to study each injection rate's, storage efficiency and temperature as presented in Eq. (9a) and (9b).

$$\Sigma V_{\text{CO}_2, \text{ in}} = \Sigma (V_{\text{CO}_2, \text{ Accumulated}} + V_{\text{CO}_2, \text{ Produced}}) \quad (9a)$$

$$\% \text{ CO}_2 \text{ Storage} = \frac{\Sigma V_{\text{CO}_2, \text{ Accumulated}}}{\Sigma V_{\text{CO}_2, \text{ in}}} \times 100 \quad (9b)$$

The higher the reservoir conditions, the more compressible CO₂ becomes, which is why most CO₂ sequestration processes are affected at CO₂ critical temperature and pressure of 31.5 °C and 74 bar, respectively (Hoteit, Fahs and Soltanian, 2019; and Godec et al., 2011). Eq. (9b) defined the proportion of CO₂ stored as the ratio of total CO₂ accumulated to that of total injected. Also, the N₂ and CO₂ gases are in their supercritical states and thus a sharp disparity in density will exist (CO₂ will have higher density owing to the special behaviour of supercritical CO₂, making it possible for the CO₂ to descend downward due to the gravity effect and simultaneously displacing the residual N₂ within the available pore spaces. Thus, a significant amount of total injected CO₂ remained trapped inside the long core, resulting in high sequestration volume.

From the range of injections and temperatures tested, the percentage CO₂ stored increases as the rate of injection increases from 0.4 – 1.2 ml/min, as seen in Table 3. For the 30 °C experimental runs, higher storage volumes were recorded at higher injection rates. At high injections, the ratio of total CO₂ injected to that of N₂ saturation was low compared to that at lower injections. This allowed most of the CO₂ within the core plug to migrate downward and be stored as the CO₂ flow stream traversed longitudinally in the core sample. The N₂ primarily acts as a retardant when in contact with CO₂, as reported in our previous works (Mohammed et al., 2019; Mohammed et al., 2021). Furthermore, the highest CO₂ storages were obtained at injection rates of 1.0 and 1.2 ml/min, resulting in 89.2 – 89.6% and 71.89 – 79.17 % for 30 and 40 °C, respectively. It can be hypothesised that CO₂ storage will be more appealing at lower temperatures as seen in the percentage storability or storage efficiency. Additionally, the plots of the differential pressure in Figs. (8d) and (e) showcase a similar trend or pattern for both temperatures, which was why both tests demonstrated a proximal range of value parameters.

On the other hand, the injection at 0.4 ml/min could not overcome the capillary forces within the narrower pore spaces of the pore matrix. This can be attributed to its density and flow progression with a characteristic differential pressure (Δp) and high permeability (k) recorded during the core flooding experiment. Thus, more of the flow paths become available for steady flow without limitation or curtailment, as seen in Eq. (10), at higher injections. Thus, the flow profile was uninterrupted, explaining the reason behind its lower longitudinal dispersion coefficient and high CO₂ storage with low mixing as expected. This agreed with the works reported by (Abba et al., 2018; Honari et al., 2016; Liu et al., 2018; Mohammed et al., 2020).

$$k = \frac{q\mu L}{A_c(\Delta P)} \quad (10)$$

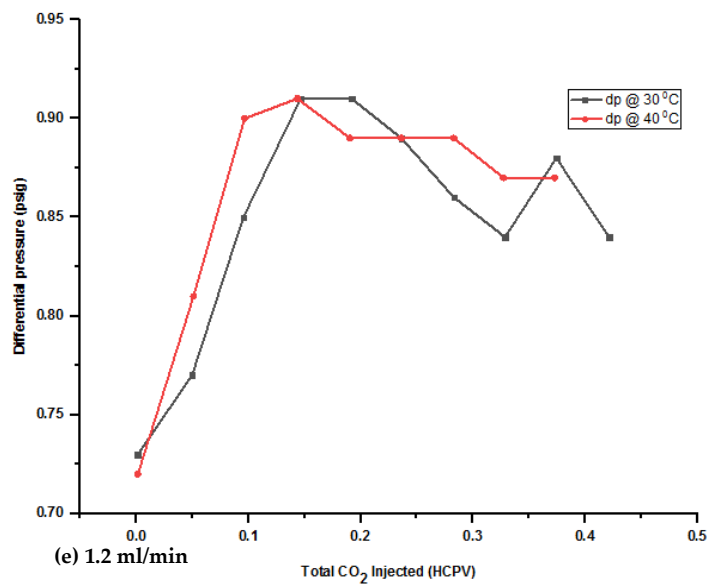
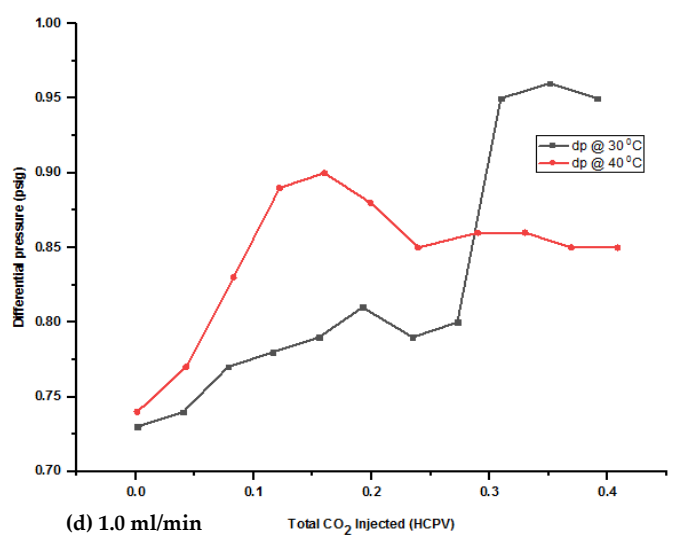
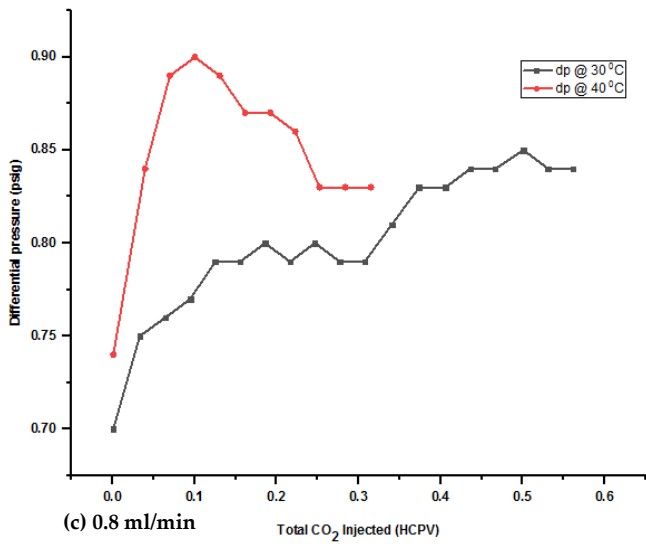
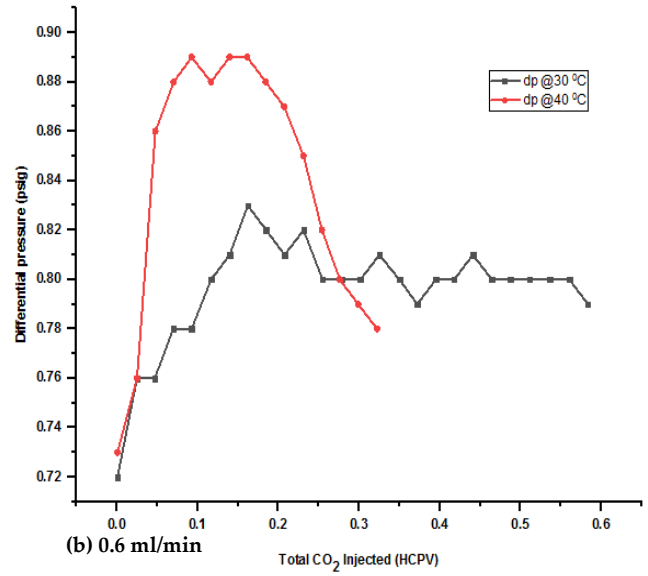
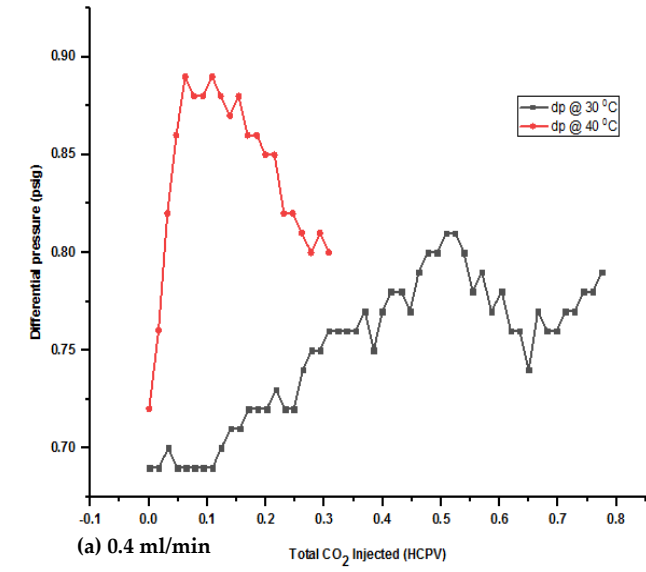


Fig. 8a-e. Differential pressure comparison for 0.4-1.2ml/min injection at 30 and 40 °C

Table 3.

General results summary at 30 and 40 °C runs

Q (ml/min)	Interstitial Velocity (10 ⁻⁵ m/s)	CO ₂ Breakthrough (HCPV)	CO ₂ Injected (HCPV)	CO ₂ Injected Stored (HCPV)	CO ₂ Stored (%)	Dispersion Coefficient (10 ⁻⁸ m ² /s)
Temp. 30 °C						
0.4	5.96	0.52	0.78	0.56	71.80	8.23
0.6	8.95	0.39	0.58	0.44	74.81	14.03
0.8	11.93	0.37	0.56	0.43	76.39	21.09
1.0	14.91	0.31	0.39	0.35	89.06	24.13
1.2	17.89	0.24	0.42	0.38	89.02	42.53
Temp. 40 °C						
0.4	5.96	0.17	0.31	0.14	46.73	12.52
0.6	8.95	0.21	0.32	0.20	61.43	17.25
0.8	11.93	0.23	0.32	0.21	66.59	25.06
1.0	14.91	0.24	0.41	0.29	71.89	33.62
1.2	17.89	0.24	0.37	0.30	79.17	39.41

5. Conclusions

This paper investigated CO₂ and N₂ behaviour using a core flooding experiment with Bentheimer as the core plug. N₂ was used as the continuous phase during the core flooding process, while CO₂ was the dispersed phase. This study is primarily designed to establish why CO₂ experiences an extended breakthrough with N₂ as the displaced gas during the displacement process. In general, the turbulence effect is undoubtedly responsible for high diffusion and dispersion along the core length due to increased flow velocities. The dispersion and diffusion coefficient increase due to temperature rise. It can be drawn that high temperature encouraged the mixing of gases under motion within the pore channel under reservoir conditions. Dispersivities for 30 and 40 °C of temperature runs were obtained as $\alpha = 0.00222$, and 0.002265 m, respectively. These values are consistent with those reported for sandstones by several researchers. Thus, higher temperatures have a more substantial effect on dispersion and diffusion coefficient, which will eventually lead to higher mixing between CO₂ and N₂. The CO₂ breakthrough tail off with reservoir temperature rise, signifying the diffusion and dispersion coefficient dependence on temperature.

The experiment at 30 °C recorded an extendable breakthrough time over that at 40 °C. The maximum breakthrough of 0.52 PV was recorded at 30 °C at the lowest injection velocity. The concentration profile plots highlighted the trend between the displacing and displaced gas during the core flooding experiment. At the 1.2 ml/min injection rate, the N₂ and CO₂ curves overlapped, and such a plot was in synergy with the breakthrough plot. Thus, it can be deduced that as the interstitial velocity increases during the EGR process, both N₂ and CO₂ experienced similar flow behaviour under reservoir conditions. From the range of injections and temperatures tested, the percentage of CO₂ stored increases as the rate of injection increases from 0.4 – 1.2 ml/min. The total CO₂ stored was more promising at higher rates, corresponding with high differential pressure, due to the flow resistance within the flow channels. Future work will aim to elucidate the effect of temperature on storage efficiency during CO₂ geological sequestration in depleted natural gas reservoirs.

Acknowledgments

We at this moment commend and appreciate the Nigerian Petroleum Technology Development Fund (PTDF) for the best scholarship award.

Nomenclature

In normal conditions, vapor is the combination of gas and liquid phases.

Gas exists in a single thermodynamic state under normal conditions.

C	Effluent composition of CO ₂
V _b	Bulk volume
SiCO ₂	Supercritical carbon dioxide
HCPV	Hydrocarbon pore volume
PV	Pore volume
EGR	Enhanced gas recovery
($\sum V_{N_2}$)	Diffusion volume of N ₂
($\sum V_{CO_2}$)	Diffusion volume of CO ₂
D	Diffusion coefficient, m ² /s
k	Permeability, mD
1AD	One-differential advection dispersion
Q	Flowrate, ml/min
t _D	Dimensionless time
x _D	Dimensionless distance
K _L	Longitudinal dispersion, m ² /s
k	Permeability, md
A	Cross section area, cm ²
L	Length of characteristic scale
ΔP	Differential pressure across the plug, atm
μ	Viscosity, cP
P	Pressure, bar
T	Temperature, °C
u	Interstitial velocity, m/s
ϕ	Core porosity, %
α	Dispersivity, m
τ	Tortuosity
P _e	Peclet number
P _{em}	Medium Peclet number

References

- Abba, M., Abbas, A., Nasr, G., Al-Otaibi, A., Burby, M., Saidu, B. and Suleiman, S., 2019. Solubility trapping as a potential secondary mechanism for CO₂ sequestration during enhanced gas recovery by CO₂ injection in conventional natural gas reservoirs: An experimental approach. *Journal of Natural Gas Science and Engineering*, 71, p.103002.
- Abba, M.K., Abbas, A.J., Athari, A., Mukhtar, A., & Nasr, G.G. (2018). Experimental Investigation on the Impact of Connate Water Salinity on Dispersion Coefficient in Consolidated Rocks Cores during EGR by CO₂ Injection. *Journal of Natural Gas Science and Engineering*, 60, 190-201. <http://doi.org/10.1016/j.jngse.2018.10.007>.

- Abba, M.K., Abbas, A.J. & Nasr, G.G. (2017). Enhanced Gas Recovery by CO₂ Injection and Sequestration: Effect of Connate Water Salinity on Displacement Efficiency. SPE Abu Dhabi International Petroleum Exhibition & Conference. <http://www.onepetro.org/doi/10.2118/188930-MS>.
- Baehr, A.L. Bruell, C.J (1990). Application of the Stefan-Maxwell Equations to Determine Limitations of Fick's Law when Modeling Organic Vapor Transport in Sand Columns. *Water Resources Research*, 26(6):1155–1163.
- Brigham, W.E., 1974. Mixing equations in short laboratory cores. *Society of Petroleum Engineers Journal* 14, 91–99.
- Coats, K.H., Whitson, C.H., Thomas, K. (2009). Modelling conformance as dispersion. *SPE Reservoir Eval. Eng.* 12, 33–47. <https://doi.org/10.2118/90390-PA>.
- Cunningham, R.E., Williams, R.J.J. (1980). *Diffusion in Gases and Porous Media*. New York: Plenum Press.
- Fuller, E. N., Schettler, P. D., and Giddings, J. C. (1966). New method for prediction of binary gas-phase diffusion coefficients, *Ind. Eng. Chem.*, 58, 18–27.
- Godec, M., Kuuskraa, V., Van Leeuwen, T., Stephen Melzer, L. and Wildgust, N., 2011. CO₂ storage in depleted oil fields: The worldwide potential for carbon dioxide enhanced oil recovery. *Energy Procedia*, 4, pp.2162-2169.
- Hoteit, H., Fahs, M. and Soltanian, M., 2019. Assessment of CO₂ Injectivity During Sequestration in Depleted Gas Reservoirs. *Geosciences*, 9(5), p.199.
- Honari, A., Hughes, T. J., Fridjonsson, E. O., Johns, M. L., & May, E. F. (2013). Dispersion of supercritical CO₂ and CH₄ in consolidated porous media for enhanced gas recovery simulations. <http://doi.org/10.1016/j.ijggc.2013.08.016>
- Honari, A., Zecca, M., Vogt, S. J., Iglauer, S., Bijeljic, B., Johns, M. L., & May, E. F. (2016). The impact of residual water on CH₄-CO₂ dispersion in consolidated rock cores. <http://doi.org/10.1016/j.ijggc.2016.04.004>
- Hughes, T. J., Honari, A., Graham, B. F., Chauhan, A. S., Johns, M. L., & May, E. F. (2012). CO₂ sequestration for enhanced gas recovery: New measurements of supercritical CO₂-CH₄ dispersion in porous media and a review of recent research. *International Journal of Greenhouse Gas Control*, 9, 457–468. <http://doi.org/10.1016/j.ijggc.2012.05.011>
- Liu, S., Zhang, Y., Xing, W., Jian, W., Liu, Z., Li, T., & Song, Y. (2015). Laboratory experiment of CO₂-CH₄ displacement and dispersion in sandpacks in enhanced gas recovery. *Journal of Natural Gas Science and Engineering*, 26, 1585–1594. <http://doi.org/10.1016/j.jngse.2015.04.021>
- Liu, S., Zhang, Y., Zhao, J., Jiang, L. and Song, Y., 2020. Dispersion characteristics of CO₂ enhanced gas recovery over a wide range of temperature and pressure. *Journal of Natural Gas Science and Engineering*, 73, p.103056.
- Liu, S.Y., Song, Y.C., Zhao, C.Z., Zhang, Y., Lv, P.F., Jiang, L.L., Liu, Y., Zhao, Y.C., 2018. The horizontal dispersion properties of CO₂-CH₄ in sand packs with CO₂ displacing the simulated natural gas. *J. Nat. Gas Sci. Eng.* 50, 293–300.
- Mamora, D.D., Seo, J.G., 2002. Enhanced recovery by carbon dioxide sequestration in depleted gas reservoirs. SPE Annu. Tech. Conf. Exhib. 1–9.
- Mesfer, M., Danish, M., Khan, M., Ali, I., Hasan, M. and Jerry, A., (2020). Continuous Fixed Bed CO₂ Adsorption: Breakthrough, Column Efficiency, Mass Transfer Zone. *Processes*, 8(10), p.1233.
- Mohammed, N., Abbas, A. and Enyi, G., 2021. The role of N₂ as booster gas during enhanced gas recovery by CO₂ flooding in porous medium. *Journal of Natural Gas Science and Engineering*, p.104051.
- Mohammed, N., Abubakar, A., Enyi, G. and Ghavami, G., 2019. Flow Characteristics Through Gas Alternating Gas Injection During Enhanced Gas Recovery. *Day 3 Wed, October 23, 2019*.
- Mohammed, N., Abubakar J. Abbas, Godpower C. Enyi, Donatus E. Edem, Salihu M. Suleiman (2020). "Enhanced Gas Recovery by Nitrogen Injection: The effects of injection velocity during natural gas displacement in

- consolidated rocks", *Journal of Natural Gas Science and Engineering*, 83, 1-14.
<https://doi.org/10.1016/j.jngse.2020.103513>
- Molly S. Costanza-Robinson and Mark L. Brusseau (2006). *Gas Transport in Porous Media*, Springer. Printed in the Netherlands, 121–132.
- Newberg, M., & Foh, S., 1988. Measurement of Longitudinal Dispersion Coefficients for Gas Flowing Through Porous Media. *SPE*, 5–9.
- Pages.mtu.edu. 2021. Mass Transport Processes. [online] Available at https://pages.mtu.edu/~reh/courses/ce251/251_notes_dir/node4.html [Accessed 19 September 2021].
- Perkins, T., & Johnston, O. (1963). A Review of Diffusion and Dispersion in Porous Media. *Society of Petroleum Engineers Journal*, 3(01), 70–84. 10.2118/480-PA
- Scanlon, B.R., Nicot, J.P., Massmann, J.M (2000). Soil Gas Movement in Unsaturated Systems. In *Handbook of Soil Science*, Sumner, M.E., ed. Boca Raton: CRC Press LLC.
- Seo, J.G., 2004. Experimental and Simulation Studies of Sequestration of Supercritical Carbon Dioxide in Depleted Gas Reservoirs. Texas A&M University.
- Seo, J.G., Mamora, D.D., 2005. Experimental and simulation studies of sequestration of supercritical carbon dioxide in depleted gas reservoirs. *J. Energy Resour. Technol.* 127, 1–6.
- Schulze-Makuch, D., 2005. Longitudinal dispersivity data and implications for scaling behavior. *Gr. Water* 43, 443–456.
- Sleep, B.E (1998). Modeling Transient Organic Vapor Transport in Porous Media with the Dusty Gas Model. *Advances in Water Resources*, 22(3):247–256.
- Takahashi, S., Iwasaki, H., 1970. The diffusion of gases at high pressures. III. The diffusion of CO₂, in the CO₂–CH₄ system. *Bulletin of the Chemical Research Institute of Non- Aqueous Solutions, Tohoku University* 20, 27–36.